Supplementary Information (SI) for Journal of Materials Chemistry A.
This journal is © The Royal Society of Chemistry 2025

Graphitic Carbon Cage Structure Encapsulating Cobalt Nanoparticles in Nitrogen-doped Biomass-derived Carbon Materials Enables High-performance Sodium-sulfur Batteries

Minghui Zhang [a,1], Shengrui Cui [a,1], Youjun Xing [a], Kang Dong [a], Haoran Li [a], Yilian Song [a], Yukui Wang [a], Dingyi Yu [a], Zengqi Zhang [b,*], Seung-Taek Myung [c,*], Yongcheng Jin [a,*]

[a] School of Materials Science and Engineering, Ocean University of China, Qingdao 266100, Shandong

[b] Qingdao Industrial Energy Storage Research Institute, Qingdao Institute of Bioenergy and Bioprocess Technology, Chinese Academy of Science, Qingdao 266101, China

[c] Department of Nanotechnology & Advanced Materials Engineering, Sejong University, Seoul 143-747, South Korea

* E-mail of corresponding authors: zhangzq@qibebt.ac.cn (Zengqi Zhang); smyung@sejong.ac.kr (Seung-Taek Myung); jinyongcheng@ouc.edu.cn (Yongcheng Jin)

1. Experimental

1.1. Sample preparation

The pine nut shells (Purchased in Hei Longjiang province of China) were first washed with up water and dried at 80 ℃ overnight in an oven. The dry pine nut shells were oxidized at 300 ℃ for 3 h in a muffle furnace, and then grind them into powder. The obtained product is the precursor of pine nut shell microporous carbon (PN). PN and $K_3[Co(CN)]_6$ (99%, Aladdin) were uniformly dispersed in 50 ml of 1 M KOH (≥ 85.0%, GR) solution with a mass ratio of 1:1 and stirred quickly for 12 h. Then, freeze-dried to remove the moisture. The obtained sample was heated at 200 ℃ for 1.5 h, 700 °C for 3 h in a tube furnace at a heating rate of 5 ℃ min^{-1} under nitrogen flow. The carbonized sample was soaked in 2 M KOH for 2 h, then washed with up water until neutral. Subsequently, it was soaked in 2 M HCl (36.0~38.0%, GR) for 2 h, washed with up water to neutrality, and dried overnight at 80 ℃ in a drying oven to obtain the sample (PN-1M-Co). Control samples etched with 0 M, 0.5 M, 1 M, and 2 M KOH solutions were prepared by the same method, except that no $K_3[Co(CN)]_6$ was added (designated as PN, PN-0.5M, PN-1M, and PN-2M, respectively).

S@PN-1M-Co was obtained by a two-step melt synthesis method.[1] High-purity sulfur (S, 99.99%, Aladdin) and PN-1M-Co were mixed in a mass ratio of 2:3, transferred into a polytetrafluoroethylene (PTFE) liner in an autoclave filled with argon, and kept at 155 ℃ for 12 h and then at 200 ℃ for 2 h and cooled to ambient temperature to form S@PN-1M-Co. The preparation process of S@PN, S@PN-0.5M, S@PN-1M, and S@PN-2M were similar to that of S@PN-1M-Co except that PN-1M-Co was replaced by PN, PN-0.5M, PN-1M, and PN-2M, respectively.

1.2. Characterization

The morphology and microstructure of the samples were characterized by using a field emission scanning electron microscope (SEM, Carl Zeiss AG, Gemini300) equipped with an energy dispersive spectroscope (EDS). XRD patterns of all samples were analyzed by a powder X-ray diffractometer (XRD, SmartLab SE, Rigaku). The surface state of the composite was characterized using X-ray photoelectron spectrometer (XPS, Thermo Scientific K-Alpha, America). Fourier transform infrared spectroscopy (FTIR, Thermo Scientific Nicolet iS10) was measured in the wavelength range of 600 cm^{-1} to 4,000 cm^{-1}. The TEM analyzed the morphology of PN-1M-Co and PN-1M. (TEM, Tecnai F20, FEI). The sulfur content was monitored by Thermogravimetric analysis (TG, HITACHI STA200, Japan) under an Ar atmosphere from 25 to 800 ℃ at a heating rate of 10 ℃ min^{-1}. The nitrogen adsorption-desorption isotherms of the samples were obtained using an Autosorb-iQ automated surface area and porosity analyzer (Quantachrome, America).

1.3. Electrochemical Measurements

The active materials, PVDF and Super-P were mixed in N-Methyl-2-pyrrolidone (NMP, 99%, Aladdin) at a mass ratio of 7:1.5:1.5 and stirred to obtain a uniform slurry. Then the prepared slurry is coated on the carbon-coated aluminum foil, vacuum-dried at 60 ℃ overnight and cut into discs with a diameter of 12 mm. The sulfur mass loading was about 1 mg cm^{-2}. CR2032 coin cells were assembled in Ar-filled glove box (H_2O and O_2 <0.01 ppm). Glass fiber (Whatman, GF/F) was used as the separator with metallic sodium as anode. The electrolyte was 1 M $NaPF_6$ in EC: DEC (1:1 vol%) with 5 wt% FEC. The amount of electrolyte added was 100 μL, and the sodium foil diameter

was 15.6 mm. The electrolyte-to-sulfur (E/S) ratio is about 30 μL mg^{-1} for a 4.93 mg sulfur cathode. The cycle performance of the cell was tested using LAND and Neware equipment with a voltage range of 0.5~2.8 V. The cycle voltammetry (CV) measurements were carried out using an electrochemical workstation (CHI 660C, China) at a selected scan rate of 0.1 mV s^{-1}. The electrochemical impedance spectroscopy experiment (EIS) was conducted over a frequency range of 0.1~10^6 Hz. The galvanostatic intermittent titration technique (GITT) was performed on LAND equipment with a 10 min current pulse at 0.1 C followed by 1 h relaxation. Electrochemical testing was conducted at a controlled temperature of 25°C unless noted otherwise.

1.4. Na_2S_6 Visualized Adsorption Tests

The Na_2S_6 solution was prepared by dissolving Na_2S and sulfur (a molar ratio of 1:5) in appropriate amount of DME and stirring at 60 °C for 6 h to form a homogeneous dark brown solution. The obtained Na_2S_6 needed to be further dilution (0.1 M) before adsorption experiments. Then, the same amount of samples were dispersed into the diluted Na_2S_6 solution and rested for 6 h. The measurement of ex situ UV−vis absorption spectra was performed after the samples (PN、PN-0.5M、PN-1M、PN-2M and PN-1M-Co) soaked in the Na_2S_6 solution for 12 h. The whole testing process was carried out in a glove box filled with argon gas.

1.5. Measurement for the Na_2S Precipitation Experiments

The Na_2S precipitation experiments were tested on the CR2032 type coin batteries. The tested electrode was prepared by PN-1M (or PN-1M-Co) with PVDF and Super-p in a mass ratio of 7:1.5:1.5 in a certain amount of NMP to obtain a uniformly mixed slurry. Then, it is coated on the carbon-coated aluminum foil and dried at 60 ℃ for 12 hours. The assembly method for testing the battery with the pure Na as anode, a glass fiber as separator, PN-1M (PN-1M-Co) electrode as cathode, Na_2S_6 solution (0.1 M, 30 μL) as electrolyte adding on the cathode side and the DME (60 μL) solvent dropped on the anode side. The batteries were first discharged galvanostatically to 1.3 V and then kept the constant potential voltage at 1.2 V until the current below 10^{-5} A.

1.6. Glass Cells Assemble and Measurement

The glass cells were assembled by using the S@PN-1M-Co and S@PN-1M electrodes as cathodes and Na metal foil as the anode. Both anode and cathode were clamped by alligator clips, and the electrolyte was 1 M $NaPF_6$ in EC: DEC (1:1 vol%) with 5 wt% FEC. Finally, the reaction vessel was sealed and taken out of the glove box for galvanostatic charge-discharge test at 0.1 C on LAND test system.

1.7. DFT calculations

All of the first principle calculations were based on the Vienna Ab initio Simulation Package (VASP).[2] The interaction between ions and valence electrons was described by Projected Augmented Wave (PAW)[3], and the exchange-correlation interaction was described by the Perdew-Burke-Ernzerhof generalized gradient approximation (PBE-GGA).[4, 5] The cut-off energy was set as 450 eV, and the convergence criteria for self-consistent electronic energy and residual force were respectively assumed to be 10^{-5} eV/atom and 0.02 eV/Å, which could ensure sufficient accuracy. A 6×6 slab with 72 atoms is employed to model graphene. A vacuum region of with a 35 Å vacuum layer was added between periodic slabs. The k points are set 1 × 1 × 1 based on Monkhorst-Pack meshes for all structures. We constructed adsorption models where Na_2S or Na_2S_6 were adsorbed on the graphene and Co7@graphene, respectively. The adsorption energy (E_{ads}) is expressed by the equation (1):

$$E_{ads} = E_{final} - E_{initial} - E_{Na2S/Na2S6}$$

where E_{final} and $E_{initial}$ refer to the energy before and after adsorption, respectively.

The electron density difference ($\Delta\rho$) is expressed by the equation (2):

$$\Delta\rho = \rho_{AB} - \rho_A - \rho_B$$

Where ρ_{AB}refer to the charge density of the complex, and ρ_A, ρ_B refer to the charge density of each fragment.

2. Result and Discussion

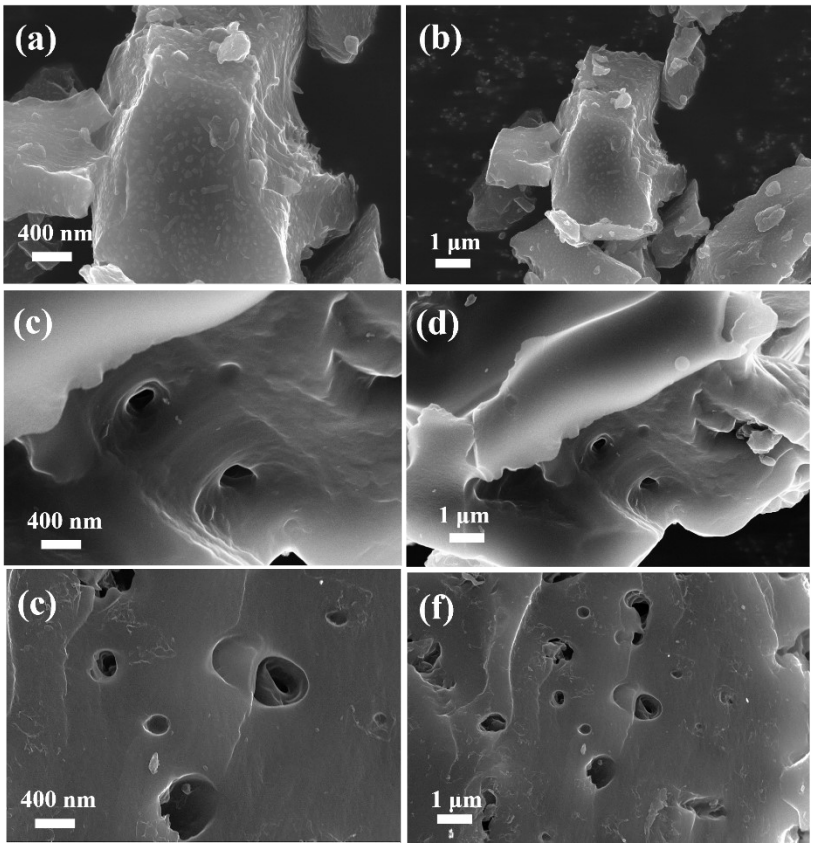

Figure S1. SEM image of (a and b) PN, (c and d) PN-0.5M, (e and f) PN-2M.

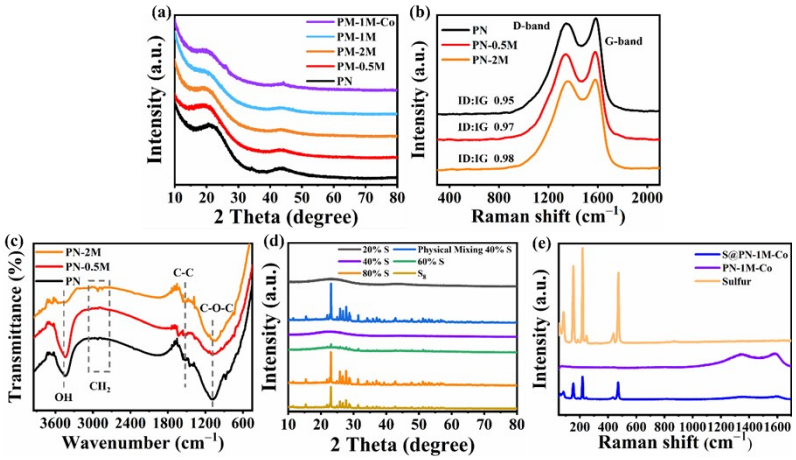

Figure S2. (a) XRD patterns of PN, PN-0.5M, PN-1M, PN-2M and PN-1M-Co. (b) Raman spectra of PN, PN-0.5M and PN-2M. (c) FTIR spectra of PN, PN-0.5M and PN-2M. (d) XRD patterns of the 20%S@PN-1M-Co, Physical Mixing 40%S@PN-1M-Co, 40%S@PN-1M-Co, 60%S@PN-1M-Co, 80%S@PN-1M-Co, and S8. (e) Raman spectra of sulfur, PN-1M-Co and S@PN-1M-Co.

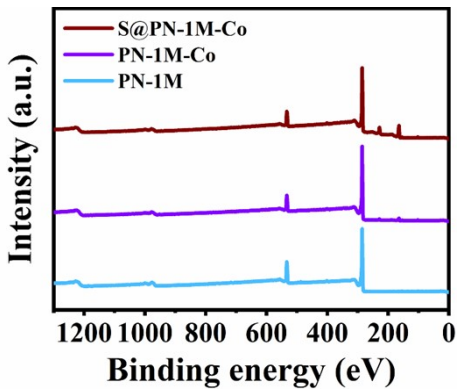

Figure S3. XPS spectra of PN-1M, PN-1M-Co and S@PN-1M-Co.

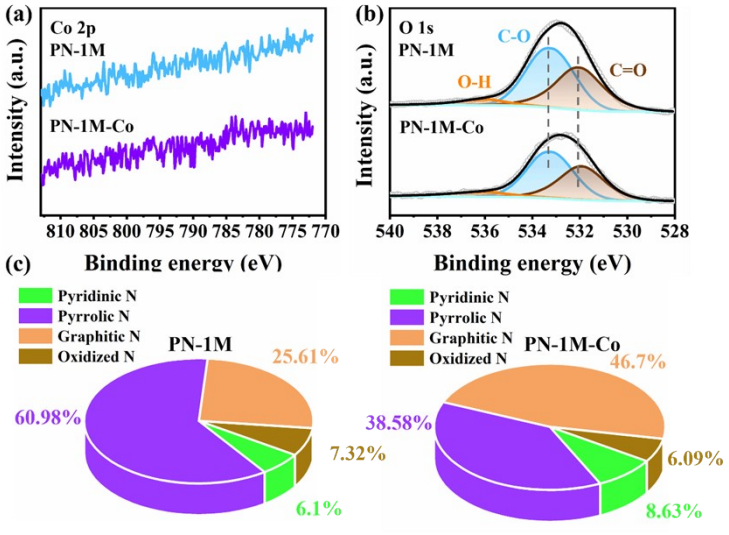

Figure S4. (a) XPS spectra of Co2p for PN-1M-Co and PN-1M. (b) XPS spectra of O1s for PN-1M-Co and PN-1M. (c) Relative proportions of different nitrogen species in PN-1M and PN-1M-Co.

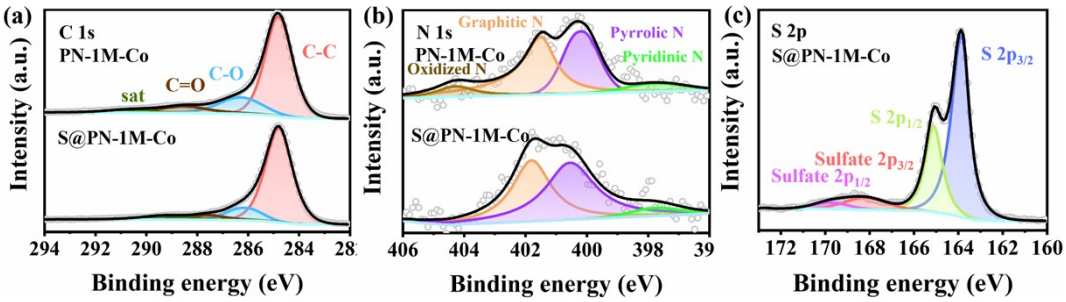

Figure S5. (a) XPS spectra of C1s for S@PN-1M-Co and PN-1M-Co. (b) XPS spectra of N 1s for S@PN-1M-Co and PN-1M-Co. (c) XPS spectra of S 2p for S@PN-1M-Co.

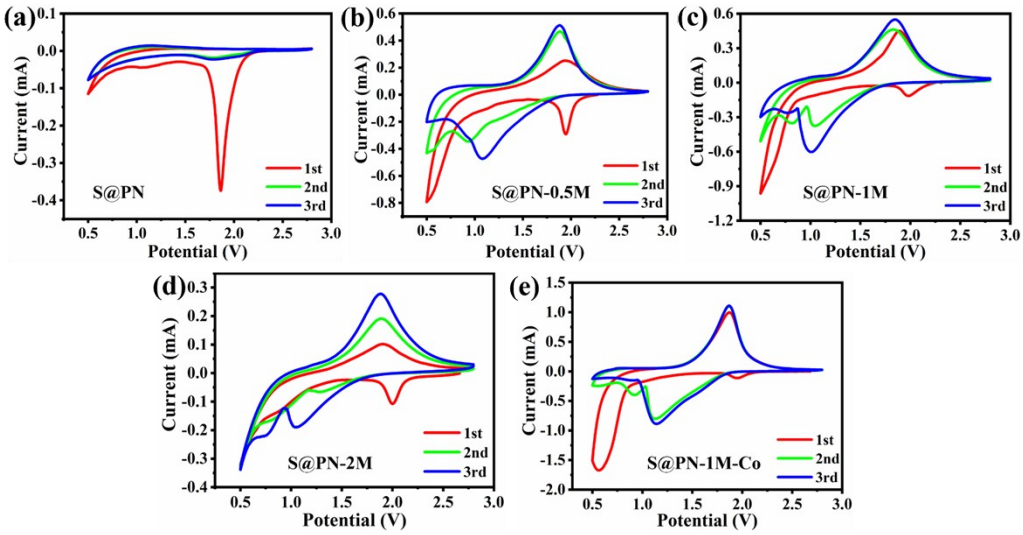

Figure S6. CV curves of (a) S@PN, (b) S@PN-0.5M, (c) S@PN-1M, (d) S@PN-2M, (e) S@PN-1M-Co.

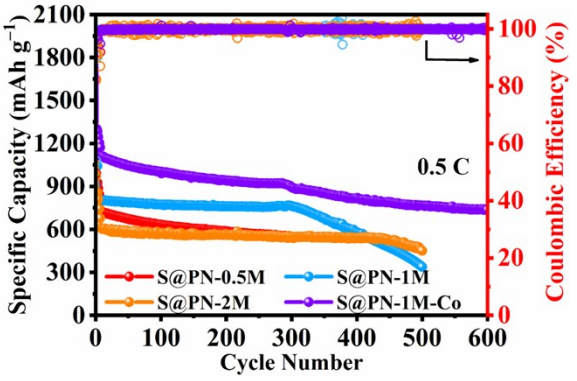

Figure S7. Cyclic performance of S@PN-0.5M, S@PN-1M, S@PN-2M and S@PN-1M-Co electrodes at 0.5 C.

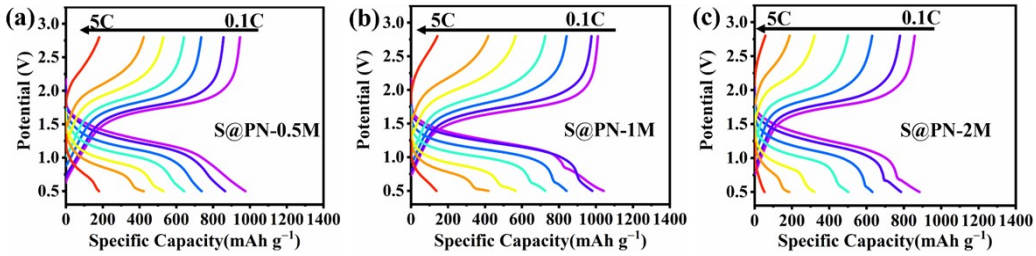

Figure S8. Charge-discharge profiles of (a) S@PN-0.5M, (b) S@PN-1M, (c) S@PN-2M at various current densities of 0.1-5 C.

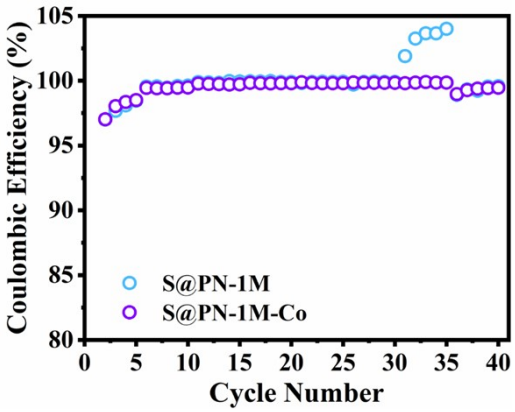

Figure S9. Coulombic efficiency of S@PN-1M and S@PN-1M-Co at 0.1, 1, 2, 3 and 5 C, respectively.

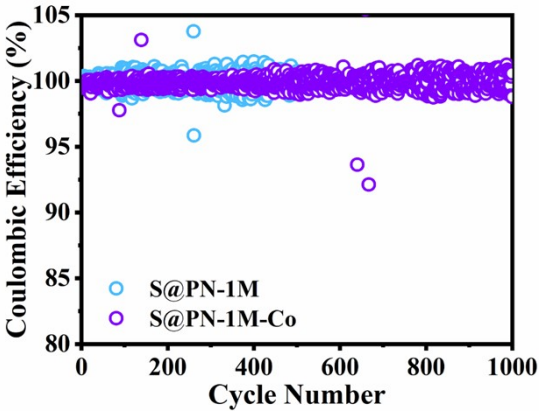

Figure S10. Coulombic efficiency of S@PN-1M and S@PN-1M-Co at 1C, respectively

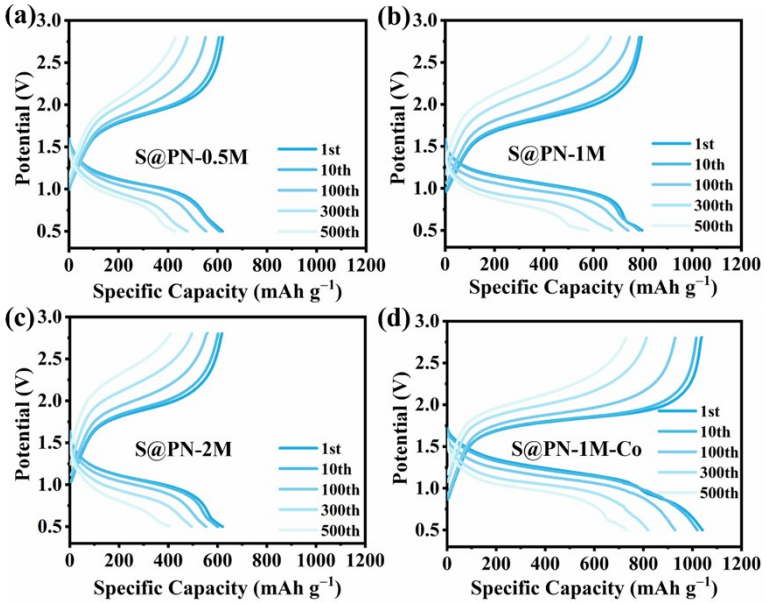

Figure S11. Charge/discharge profiles of (a) S@PN-0.5M, (b) S@PN-1M, (c) S@PN-2M and (d) S@PN-1M-Co at 1.0 C.

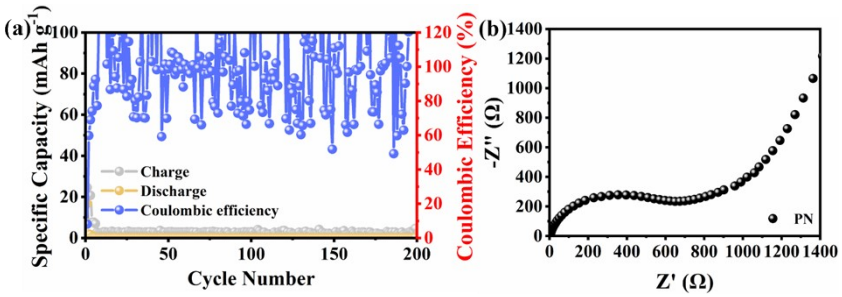

Figure S12. (a) Cyclic performance of S@PN electrodes at 1.0 C. (b) EIS Nyquist plot of S@PN after measurement of rate performance (discharge state).

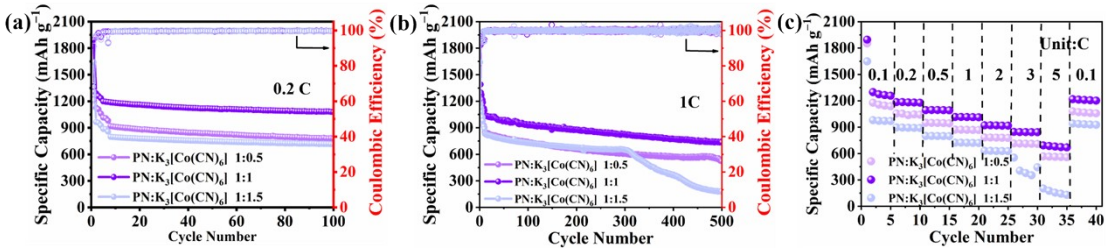

Figure S13. Cyclic performance at different $K_3[Co(CN)_6]$ proportions. (a) 0.2C, (b) 1C. (c) Rate performance at different current densities.

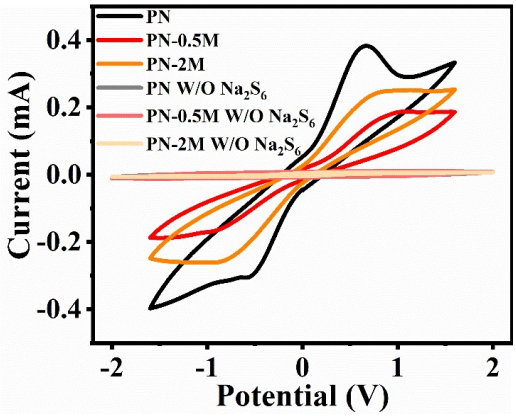

Figure S14. CV curves of symmetrical cells with PN, PN-0.5M and PN-2M.

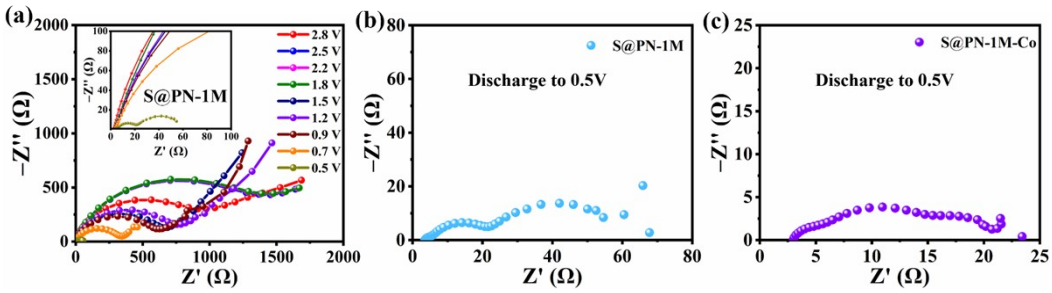

Figure S15**.** (a) In situ EIS of the S@PN-1M during the discharge process. (b) Nyquist plot of S@PN-1M during discharge to 0.5V. (c) Nyquist plot of S@PN-1M-Co during discharge to 0.5V.

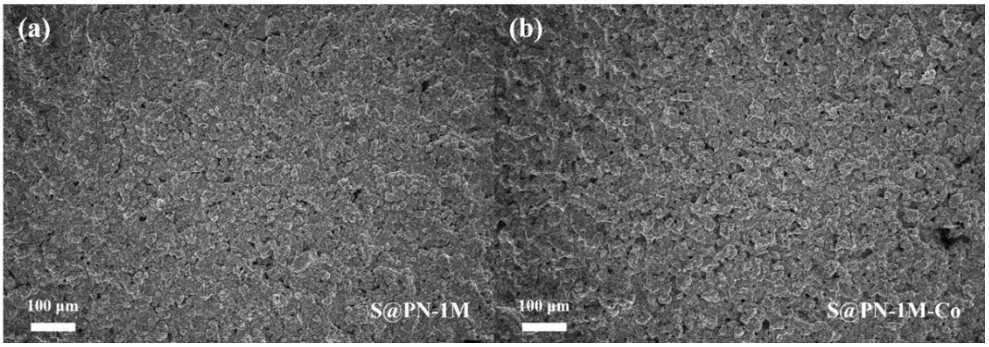

Figure S16. SEM images of (a) S@PN-1M, (b) S@PN-1M-Co pristine cathodes.

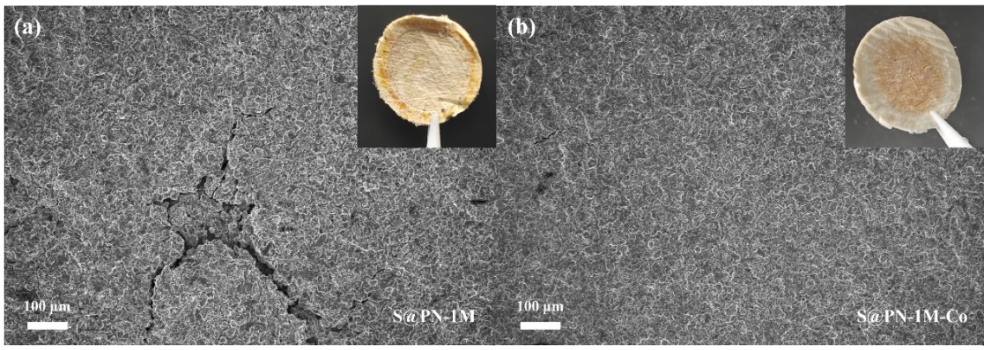

Figure S17. SEM images of (a) S@PN-1M, (b) S@PN-1M-Co cathodes after 500 cycles at 1C. The inset is the separators corresponding digital photo.

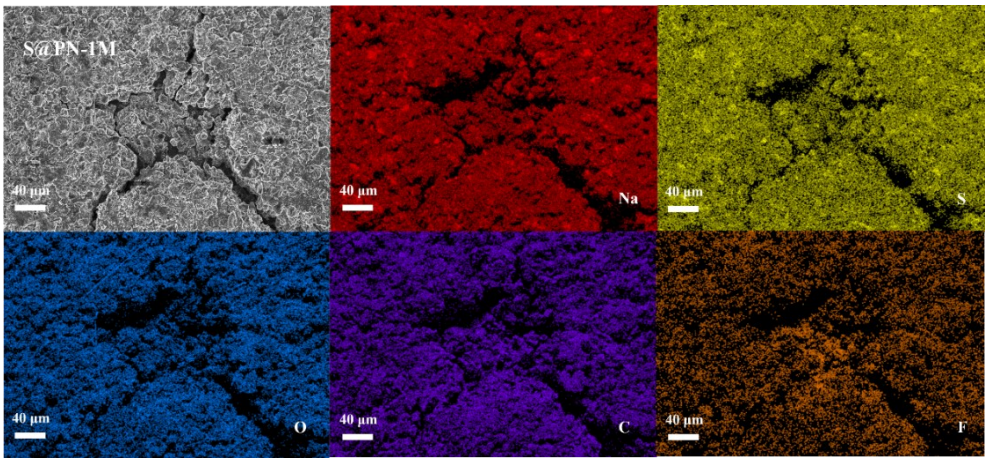

Figure S18. SEM image of S@PN-1M cathode and corresponding EDS mappings of C, O, F, S and Na elements after 500 cycles at 1C.

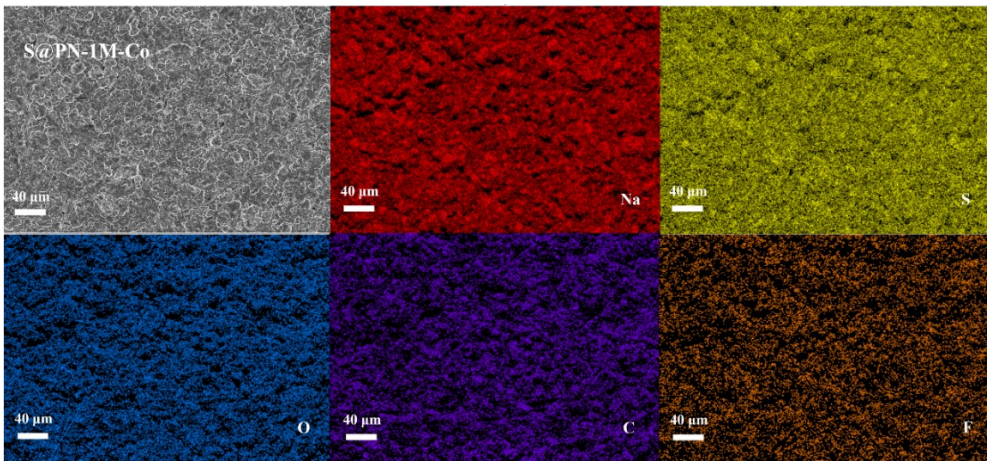

Figure S19. SEM image of S@PN-1M-Co cathode and corresponding EDS mappings of C, O, F, S and Na elements after 500 cycles at 1C.

Table S1. Cathode composition and electrochemical performance of the battery in this work to various cathodes reported in previous literature.

Cathode	Capacity at 0.1C	Capacity at 0.2C	Capacity at 0.5C	Capacity at 1.0C	Capacity at 2.0C	Capacity at 3.0C	Capacity at 5.0C	Sulfur loading density (mg/cm^2)	Ref
S@PN-1M-Co	1264.7	1182.3	1094.5	1014.7	919	843.5	679.6	1.0	This work
WBMC@S	1286.5	1077	795	601	/	472	/	1.0	6
S@CNT/NPC	866	756	640	454	/	/	/	/	7
S@NPC-700	800	686	618.8	496	280.9	/	/	0.7	8
CN/Au/S	830	755	678	599	/	/	/	0.9	9
APCF-38S	1074	919	726	600	374	/	/	/	10
S/YS-Fe_2N@NC	/	/	725	620	488	422	/	/	11
S/phos-C	1034	938	809	711	568	/	/	/	12
RGO/SiO_2/S	750	586	320	185	/	/	/	0.79	13
S@Co/C/rGO	461	209	164	150	/	/	/	/	14
S@WCG	1154	/	903	712	/	/	/	0.7~0.8	15
2D/3D Co_4N-NC@CC-S	/	/	823	711	528	466	/	/	16

Reference

1. Z. Shi, T. Wang, Z. Shi, S. Cui, Z. Zhang, W. Liu and Y. Jin, *Chem. Eng. J.*, 2023, **457**, 141264.
2. G. Kresse and J. Furthmüller, *Physical Review B*, 1996, **54**, 11169-11186.
3. P. E. Blöchl, *Physical Review B*, 1994, **50**, 17953-17979.
4. J. P. Perdew, K. Burke and M. Ernzerhof, *Phys. Rev. Lett.*, 1996, **77**, 3865-3868.
5. J. P. Perdew, K. Burke and Y. Wang, *Physical Review B*, 1996, **54**, 16533-16539.
6. D. Zhao, S. Ge-Zhang, Z. Zhang, H. Tang, Y. Xu, F. Gao, X. Xu, S. Liu, J. Zhou, Z. Wang, Y. Wu, X. Liu and Y. Zhang, *ACS Appl. Mater. Interfaces*, 2022, **14**, 54662-54669.
7. T. Yang, W. Gao, B. Guo, R. Zhan, Q. Xu, H. He, S.-J. Bao, X. Li, Y. Chen and M. Xu, *Journal of Materials Chemistry A*, 2019, **7**, 150-156.

8. J. Mou, T. Liu, Y. Li, W. Zhang, M. Li, Y. Xu, J. Huang and M. Liu, *Journal of Materials Chemistry A*, 2020, **8**, 24590-24597.
9. N. Wang, Y. Wang, Z. Bai, Z. Fang, X. Zhang, Z. Xu, Y. Ding, X. Xu, Y. Du, S. Dou and G. Yu, *Energy & Environmental Science*, 2020, **13**, 562-570.
10. Q. Guo, S. Sun, K.-i. Kim, H. Zhang, X. Liu, C. Yan and H. Xia, *Carbon Energy*, 2021, **3**, 440-448.
11. M. K. Aslam, T. Hussain, H. Tabassum, Z. Wei, W. Tang, S. Li, S.-j. Bao, X. S. Zhao and M. Xu, *Chem. Eng. J.*, 2022, **429**, 132389.
12. Y. Wang, Y. Wang, C. Xu, Y. Meng, P. Liu, C. Huang, L. Yang, R. Li, S. Tang, J. Zeng and X. Wang, *ACS Nano*, 2024, **18**, 3839-3849.
13. Samriddhi, A. Patel, A. Tiwari, S. P. Singh, V. Yadav, R. K. Tiwari and R. K. Singh, *Journal of Energy Storage*, 2024, **99**, 113260.
14. Q. Ma, G. Du, B. Guo, W. Tang, Y. Li, M. Xu and C. Li, *Chem. Eng. J.*, 2020, **388**, 124210.
15. Y. Liu, D. J. Lee, H.-J. Ahn, S. Y. Nam, K.-K. Cho and J.-H. Ahn, *Renewable Energy*, 2023, **212**, 865-874.
16. Y. Li, X. Wang, M. Sun, L. Ai, L. Qin, Z. Zhao and J. Qiu, *Electrochim. Acta*, 2023, **451**, 142288.